# High-performance tapered fiber surface plasmon resonance sensor based on graphene/Ag/TiO2 layer

**Dan Wang**
NJUPT
**Wei Li** ( liw@njupt.edu.cn )
NJUPT https://orcid.org/0000-0001-9120-3345
**Qingrong Zhang**
NJUPT
**Benquan Liang**
NJUPT
**Zhenkai Peng**
NJUPT
**Jie Xu**
njupt
**Chen Zhu**
NJUPT
**Jinze Li**
NJUPT

**Research Article**

**Keywords:** Surface plasmon resonance, Micro-fiber, Graphene/Ag/TiO2, Sensor

**Posted Date:** March 26th, 2021

**DOI:** https://doi.org/10.21203/rs.3.rs-344763/v1

# High-performance tapered fiber surface plasmon resonance sensor based on graphene/Ag/$TiO_2$ layer

Dan Wang[1,4], Li Wei[1,2,3,4*], Qinrong Zhang [1,4], Benquan Liang [1,4], Zhenkai Peng [1,4], Jie Xu[1,4], Chen Zhu[1,4], Jinze Li[1,4]

[1)] (College of Electronic and Optical Engineering and College of Microelectronics, Jiangsu Optical Communication Engineering Technology Research Center, Nanjing Universuty of Posts and Telecommunications, Nanjing 210023, China)

[2)] (State Key Laboratory of Luminescent Materials and Devices, South China University of Technology, Guangzhou 510641, China)

[3)] (State Key Laboratory of Bioelectronics, Southeast University, Nanjing 210096, China)

[4)] (Jiangsu Province Engineering Research Center for Fabrication and Application of Special Optical Fiber Materials and Devices, Nanjing 210093, China)

**Abstract**: In this paper, a highly sensitive surface plasmon resonance sensor is proposed on the basis of a miniature tapered single-mode fiber. The sensing area of the tapered fiber is coated with graphene, silver and titanium dioxide layer. The graphene layer is used to increase the light absorption rate, and the titanium dioxide layer is used to protect the silver layer from oxidation and improve the sensor sensitivity due to its high dielectric constant. And optimizing the thickness of graphene, silver and titanium dioxide layer. According to the simulation calculation results, when the graphene is 15 layers, the silver layer is 40 nm, and the titanium dioxide is 20 nm, high-performance SPR can be obtained. The sensor has a detection range of 1.32-1.38, and its sensitivity can reach 8750 nm/RIU when the external refractive index is 1.38. The research results have potential application value for the design of high-performance SPR sensors.

**Keywords**: Surface plasmon resonance, Micro-fiber, Graphene/Ag/$TiO_2$, Sensor

*Corresponding author. E-mail: Liw@njupt.edu.cn*Liw@njupt.edu.cn

## 1. Introduction

Surface plasmon resonance (SPR) is a common optical physical phenomenon, which is caused by the coupling oscillation between photons and free electrons on metal surface, and is particularly sensitive to the medium on the metal surface. Therefore, SPR substance detection technology have been widely used and researched deeply in the fields of chemistry, biology and medicine due to their high sensitivity, no labeling, and real-time detection[1-3].

The Kretschmann[4] prism coupling structure is a more traditional way to stimulate SPR, but the sensor based on the prism structure has the disadvantages of large volume, complex system, and long-distance transmission, which limits its practical application. In 1993, Jorgenson and Yee of the University of Washington in the United States combined optical fiber with SPR technology, based on the principle of attenuated total reflection(ATR), successfully designed an optical fiber SPR sensor[5]. Comparing with the Kretschmann prism structure, the optical fiber SPR sensor has the advantages such as small size, high resolution, and anti-electromagnetic interference. Since then, the optical fiber SPR sensor has been extensively studied. Its main research direction is the design of fiber structure and the choice of coating for optical fiber sensing area. So far, many fiber structures have been proposed to realize microstructure fibers, including single-mode fiber(SMF)[6,7], multi-mode fiber(MMF)[8,9], photonic crystal fiber(PCF)[10,11],polarization maintaining fiber[12], plastic polymer fiber[13], hollow core fiber[14], etc. However, the MMF supports a large number of transmission modes, which will widen the full width at half maximum(FWHM), thereby reducing the detection accuracy of the sensor, the PCF is costly and difficult to manufacture, and the polarization maintaining fiber, plastic fiber and hollow fiber are in the research stage due to their unique properties. SMF has a relatively simple structure and narrow FWHM, so it is usually used to construct SPR sensors. In order to excite SPR, the metal coating of the sensing area usually uses precious metals, such as gold and silver. Since the imaginary part of the dielectric constant of the silver film is larger than that of the gold film, and the real part is smaller than that of the gold film, the FWHM and sensitivity of the silver film

sensor are smaller than that of the gold film. In this paper, silver film is selected as the metal layer that excites SPR. However, silver is unstable in air, which will affect the performance of the sensor. Therefore, the silver surface is usually coated with a high dielectric constant adjusting layer (such as $TiO_2$[15], ZnO[16,17]), which can not only prevent the silver layer from being oxidized, but also improve the electric field strength between the upper oxide layer and the sensing medium, so as to improve the sensitivity of the sensor. $TiO_2$ has been widely used because it has a stronger binding to light than other oxide dielectrics[18,19] Two-dimensional materials (graphene, $Ws_2$, $Wse_2$, $Mos_2$, $Mose_2$)[20-23] have also been extensively studied as coating in SPR sensing due to their unique properties, especially graphene, because the absorptivity of single-layer graphene is about 2.3%, the absorptivity of graphene increases as the number of layers, and the light transmittance of graphene is as high as 97.7%[24,25]. Based on the excellent properties of graphene can be used to improve the sensitivity of the sensor. F.M. Wang et al. proposed a photonic crystal fiber SPR sensor based on silver/graphene structure to improve the performance of the sensor[26]. A U-shaped optic fiber SPR biosensor based on the graphene/AgNPs is presented by C. Zhang, et al. which experimental results show that graphene layer can improve the sensitivity of the sensor[27]. Jeeban Kumar Nayak et al. covered the D-type surface with silver and graphene, and the sensitivity could reach 6800 nm/RIU[28]. All the above studies show that graphene has important applications in improving the performance of sensors.

So far, the most research on the single-mode fiber is the D-type side-polished fiber[29]. The evanescent wave of the core is revealed by polishing off the cladding of a certain thickness. Due to the fragility of the optical fiber, a high degree of controllability is required in the process of manufacturing D-type optical fiber, so the requirements for experiments are particularly high. The research in this paper is based on a cylindrical tapered single-mode fiber. The tapered fiber is divided into a sensing area and a taper transition region, which can be made by mechanical tapering or chemical etching[30,31]. This paper theoretically studies the SPR tapered single-mode sensor with graphene/silver/titanium dioxide coating, and optimizes the parameters of each coating layer.

## 2. Sensor structure and theoretical modelling

Fig.1 shows the structure diagram and cross-sectional view of the tapered single-mode fiber proposed in this article. When the fundamental mode in the single-mode fiber is transmitted to the tapered sensing region, the mode field diameter is reduced due to the reduction of the fiber diameter, so that a part of the fundamental mode is coupled to the outside of the cladding to form evanescent wave and generate evanescent field. Due to the effect of evanescent field, a surface plasmon waves(SPW) is generated at the interface between metal and sensing medium. When the wave vectors of the evanescent wave and SPW are equal in the x-direction, the phase matching condition is met, and the oscillating free electrons absorb part of the transmitted light energy, resulting in an absorption peak in the resonance transmission spectrum. The dispersion formula of SPW is:

$$\beta = k\sqrt{\frac{\varepsilon_s \varepsilon_m}{\varepsilon_s + \varepsilon_m}} \tag{1}$$

where k is the number of free-space wave vectors, $\varepsilon_s (\varepsilon_s = n_s^2)$ is the dielectric constant of the analyte, and $\varepsilon_m$ is the dielectric constant of the metal. The SPW wave vector changes with the dielectric constant of the analyte, causing the resonance wavelength of the SPR to shift. Therefore, we can detect the refractive index of the analyte by detecting the change in resonance wavelength.

In this simulation calculation, the cladding diameter of the sensing area is set to 7.25 $\mu m$, the core diameter is 5.25 $\mu m$, the refractive index of the cladding and core are 1.4378 and 1.4438 respectively, and the length of the sensing area is 0.1 mm. The dielectric constant of is written as follows according to the Drude model[32]:

$$\varepsilon_m(\lambda) = 1 - \frac{\lambda^2 \lambda_c}{\lambda_p^2 (\lambda_c + i\lambda)} \tag{2}$$

where $\lambda_c$ is the plasma wavelength, $\lambda_p$ is the collision wavelength, they are $1.7614 \times 10^{-5} m$ and $1.4541 \times 10^{-7} m$ respectively. The dielectric constant of the dielectric layer $TiO_2$ can be written as[33]:

$$\varepsilon_{TiO_2} = n_{TiO_2}^2 = 5.913 + \frac{0.2441}{(\lambda^2 - 0.0803)} \quad (3)$$

where $\lambda$ is the incident light wavelength, the unit is millimeters.

The refractive index of graphene is[34]:

$$n_g = 3 + i\frac{C_1}{3}\lambda \quad (4)$$

where λ is the vacuum wavelength, $C_1 = 5.446\mu m$. The thickness of a single-layer graphene is 0.34 nm, when the number of graphene layers is N, its thickness is $d = 0.34 \times N$ nm. The transmittance is expressed as:

$$T(\lambda) = \exp(-\frac{4\pi}{\lambda}\mathrm{Im}(n_{eff})L) \quad (5)$$

where $n_{eff}$ represents the effective refractive index of the surface plasmon mode, Im represents its imaginary part, and L is the length of the sensing area. An important parameter that characterizes the performance of a sensor is sensitivity, which can be expressed as the ratio of resonance drift to the change in refraction of the analyte:

$$S_\lambda(\lambda)(nm/RIU) = \frac{\Delta\lambda}{\Delta n} \quad (6)$$

Another important sensor performance parameter is the FWHM, which refers to the difference between the corresponding maximum and minimum wavelengths when the resonance absorption peak is attenuated by half. The figure of merit (FOM) is the ratio of sensitivity to FWHM:

$$FOM = \frac{S}{FWHM} \quad (7)$$

FOM is a comprehensive parameter of sensor performance. It can be seen from the equation (7), the FOM is directly proportional to the sensitivity and inversely proportional to FWHM.

In the simulation calculation of this article, the cross-section of the tapered optical fiber sensing area is modeled. When the SPR effect is generated, the electric field intensity distribution of the cross section is shown in Fig.2(a). Fig.2(b) is a graph

of electric field amplitude changing with radians. When the SPR effect occurs, the energy on the two sides of the cross-section symmetry is locally strengthened, rather than the energy at the interface of the entire circle. This is because only p-polarized light can produce SPR, and s-polarized light does not produce SPR.

## 3. Results and discussion

### 3.1. Silver film sensor

In order to optimize and determine the thickness of the Ag film. The thickness of the silver film is set to 20 nm, 30 nm, 40 nm, 50 nm, 60 nm and 70 nm, and the external refractive index is 1.37 . The simulated transmittance spectrum is shown in Fig.3. It can be seen from Fig.3 that the resonance peak appears red-shifted as the thickness of the silver film increases. But when the thickness of silver is less than 40 nm, the shift of resonance wavelength is more sensitive to the thickness of silver, and the transmission depth gradually becomes deeper as the thickness of Ag increases, but when the thickness of Ag exceeds 40 nm, the resonance shift is gradually decrease, when the Ag thickness is 60 nm, 70 nm, the resonance peak is almost unchanged, and the resonance depth gradually becomes shallower as the Ag thickness increases. The reason is that the thickness of the silver layer is too large, which will reduce the evanescent wave penetrating the metal layer, resulting SPW and evanescent wave energy coupling to decrease, which in turn leads to the reduction of the intensity of the SPR peak. Therefore, the thickness of Ag is maintained at 40 nm, which has a good SPR spectrum. Fig.4(a) is the transmission spectrum of the refractive index of the sensing area from 1.32 to 1.38. It can be seen from the figure that as the sensing refractive index continues to increase, the resonance wavelength red-shift, and the transmission depth is increasing. Fig.4(b) is the fitting curve of the resonance wavelength with the change in refractive index. The fitting coefficient $R^2$ is 0.99956. It can be seen from this figure that when the refractive index is 1.36, 1.37 and 1.38, the sensitivity reaches 3640.47 nm/RIU, 4159.5 nm/RIU, 4678.57 nm/RIU, respectively.

### 3.2. Fiber- graphene- silver film sensor

Add a layer of graphene between the optical fiber and the metal layer of silver. Since graphene has light absorption and semi-metal properties, using this feature can enhance the sensitivity of the sensor. The thickness of metallic silver is 40 nm. Fig.5 shows the variation of resonance peaks with the number of graphene layers under different refractive index of analytes. It can be seen that as the thickness of the graphene increases, the resonance peak shift-red, and the slope of the resonance curve represents the sensitivity of the sensor. Fig.5(b) shows the change of sensitivity and FWHM with the number of graphene layers when the external refractive index is 1.37. It can be seen that both the sensitivity and FWHM increase with the number of graphene layers. But the increase in FWHM leads to a decrease in the detection accuracy of the sensor. Table 1 shows the specific values of sensitivity, FWHM, and quality factor varying with the number of graphene layers when the refractive index of analyte is 1.37. Considering the influence of graphene on the quality factor and sensitivity of the sensor, 15 graphene layers are selected in the later simulation. For graphene with 0 layers and 15 layers, the refractive index is 1.32-1.38, and its sensitivity is shown in Table 2. It can be seen from the table that the sensitivity of the sensor with the graphene layer has been improved.

### 3.3 Fiber-graphene-silver-$TiO_2$ film sensor

Since silver as the outermost layer is easily oxidized and affects the stability of the sensor, it can be considered to cover the outer surface of silver with $TiO_2$, a material with high dielectric constant. Fig.6 shows the curve of the SPR resonance spectrum varying with the thickness of the $TiO_2$ when the outer layer of the optical fiber has been coated with 15-layer graphene/40 nm Ag and the analyte refractive index is 1.37. It can be seen from Fig.6(a) that as the thickness of $TiO_2$ increases, the resonance peak moves to the long wave direction and the FWHM gradually widens. The maximum transmission depth is when $TiO_2$ is 5 nm. It can be seen from

Fig.6(b)(c) that FWHM exists when the thickness of $TiO_2$ is 20 nm, but when $TiO_2$ is greater than 20 nm, FWHM no longer exists. Therefore, when the thickness of $TiO_2$ reaches 25 nm, it is no longer suitable for sensors. Fig.7 shows that the SPR resonance peak varies with the refractive index of the analyte under different thicknesses of $TiO_2$. It can be seen from from the figure that when the thickness of $TiO_2$ is the same, the resonance peak shifts to the long wave direction with the increase of the refractive index. When the external refractive index unchanged, the resonance peak red-shifts as the thickness of $TiO_2$ increases. We can see that the relationship between the resonance wavelength and the refractive index of the analyte is nonlinear. The obtained data points are fitted by a quadratic polynomial, and the slope of each point is used to characterize the sensor sensitivity. The relationship between sensitivity and refractive index change is shown in Fig.8. When the refractive index of the analyte is 1.38, the sensitivity changes with the thickness of $TiO_2$ are 5021.4 nm/RIU, 5785.7 nm/RIU, 7578.5 nm/RIU, 7579.0 nm/RIU, 8570 nm/RIU, respectively. In general, the sensitivity of the SPR sensor basically increases with the thickness of $TiO_2$. The graphene/Ag/$TiO_2$ structure of the single-mode tapered fiber SPR sensor designed in this paper has advantages in sensitivity compared with other structures, as shown in Table 3.

3.4. System analysis

In order to systematically analyze how each layer of material affects the performance of the SPR sensor, the simulation diagram is shown in Fig9. Table 4 shows the specific values of sensitivity and FWHM of each structure. Fig.9(a) shows the SPR transmission spectrum when the tapered single-mode fiber is only coated with Ag. When the refractive index of the analyte is 1.36, the resonance peak shift and FWHM are 60 nm and 14 nm, respectively, the sensitivity is about 3000 nm/RIU. which indicates that the sensitivity of the sensor with only one layer of Ag is not very high. Fig.9(b) is the transmission spectrum when 15 layers of graphene are coated between the silver film and the optical fiber. The resonance drift about 64 nm. The sensitivity is 3200 nm/RIU, and the FWHM is 20 nm. Compared with no graphene layer, the sensitivity and FWHM are slightly increased. Fig.9(c) shows the reflection

curve of the Ag/$TiO_2$ sensor. From figure we can see that the resonance peak shift and FWHM is greatly increased compared with the sensor with 40 nm Ag film and 15-layer graphene/40 nm Ag structure, the sensitivity is about 4800nm/ RIU and the FWHM is 115nm when refractive index of analyte is 1.36. Fig.9(d) is the reflection resonance curve of a 15-layer graphene/40 nm Ag/20 nm $TiO_2$ sensor. It can be seen from Table 4 that the sensitivity of the sensor with this structure is about 5000 nm/RIU, and the FWHM is 84 nm. The sensitivity of the graphene/Ag/$TiO_2$ structure sensor is greatly improved compared with the graphene/Ag, and the FWHM is narrower than the Ag/$TiO_2$. In the comparison of structures c and d, it can be seen that the addition of graphene reduces the FWHM of the sensor and the sensitivity slightly increases. Comparing structures b and d, we can know that $TiO_2$ greatly improves the sensitivity of the sensor.

3.5. Optical field distribution of fiber SPR sensor

In order to analyze how each layer of material affects the electric field intensity distribution of the SPR sensor. Fig.10 shows the TM polarization electric field intensity distribution and electric field amplitude distribution diagram when the analyte refractive index is 1.32 with different sensor structures. Fig10(a) shows that the sensor structure is 40 nm Ag, and its electric field is locally enhanced at a symmetrical position, and SPR phenomenon occurs. Fig.10(b) shows the electric field distribution of 15-layer graphene/40 nm Ag structure. It can be seen from the figure that the electric field intensity at the core and sensor interface is much higher than that of the 40 nm Ag sensor. This is because the light absorption of graphene promotes the excitation of surface plasmon resonance. Simultaneously, because graphene is a zero-gap semiconductor, its carrier concentration can be as high as $10^{13}cm^{-2}$, and it has no mass, no scattering, and extremely high mobility[36,37]. Therefore, the existence of graphene promotes the transmission of photons, so that more photons are transfer to the silver film to increase the surface electric field intensity. The sensor based on the graphene/silver structure greatly improves the performance of the sensor. Fig.10(c) is the electric field intensity distribution curve of the 15-layer graphene/40 nm Ag/20

nm $TiO_2$ structure. It can be seen from the figure that most of the energy is coupled to form an evanescent wave to excite SPW, and only a small part of the energy continues to be transmitted in the core in the form of the fundamental mode. Due to the translucency of $TiO_2$ in visible light and near-infrared light and can transfer the dielectric layer electrons to the metallic silver film, thereby greatly increasing the resonance energy coupling. Fig.11 is the electric field intensity distribution diagram of the graphene/Ag/$TiO_2$ SPR sensor under different analyte refractive index. We can see from the figure that the electric field intensity of interface coupling increases with the refractive index of analyte, which means that the sensor becomes more sensitive with the increase of refractive index. The sensitivity of the sensor improve with the increase of refractive index.

## 4. Conclusion

This paper proposes a single-mode tapered fiber SPR sensor with graphene/silver/$TiO_2$ coatings, and optimizes its parameters. The detection range of the sensor is 1.32 to 1.38, and the sensitivity can reach 8570 nm/RIU when the refractive index is 1.38. Simultaneously, systematically analyzed and compared the performance of four SPR sensors with different structures: Ag, graphene/Ag, Ag/$TiO_2$, graphene/Ag/$TiO_2$, and found that the overall performance of the sensor with the last structure is the best. The electric field intensity and amplitude distribution of sensors with several different structures have also been studied, showing that graphene and $TiO_2$ can indeed enhance the electric field coupling strength of the SPR sensor and enhance the performance of the sensor. According to the research results of this article, it has theoretical guiding significance for manufacturing high-performance SPR sensors.

# Funding

This work was supported by Natural Science Research Projects of Jiangsu Province University (20KJA510001), China Postdoctoral Science Foundation (2018T110480), Open Foundation of State Key Laboratory of Luminescent Materials and Devices (2020-skllmd-03), Research Center of Optical Communications Engineering & Technology, Jiangsu Province (ZXF201904), and Open Foundation of State Key Laboratory of Bioelectronics, Southeast University.

Authors Contributions：Dan Wang and Wei Li conceived the idea. Chen Zhu and Jie Xu developed the theory. Qinrong Zhang and Jinze Li performed the simulation. Dan Wang , Benquan Liang and Zhenkai Peng analyzed the data and wrote the manuscript.

Data Availability: All data that support the findings of this study are available from the corresponding author upon reasonable request.

Compliance with Ethical Standards

Competing Interests: The authors declare that they have no competing interest.

Consent to Publish: All authors agree to publish these papers.

Ethical Approval: Not applicable.

Consent to Participate: Not applicable.

## References

[1] Y. Zhao, M. Lei, S.X. Liu, et al., Smart hydrogel-based optical fiber SPR sensor for pH measurements, Sensors and Actuators B Chemical. 261 (2018) 226-232.

[2] W.J. Wang, Z.G. Mai, Y.Z. Chen, et al., A lable-free fiber optic SPR biosensor for specific detection of C-reactive protein, Scientific reports. 7 (2017) 16904.

[3] S. Zeng , D. Baillargeat , H.P. Ho , et al., Nanomaterials enhanced surface plasmon resonance for biological and chemical sensing applications, Chemical Society Reviews. 43 (2014) 3426-3452.

[4] E. Kretschmann, H. Raether, Radiative decay of non-radiative surface plasmons excited by light. Zeitschrift fur Naturforschung, 23 (1968) 2135-2136.

[5] R.C. Jorgenson, S.S. Yee, A fiber-optic chemical sensor based on surface plasmon resonance, Sensors & Actuators B Chemical. 12(1993) 213-220.

[6] M.D. Baiad, R. Kashyap, Concatenation of surface plasmon resonance sensors in a single optical fiber using tilted fiber Bragg gratings, Optics Letters. 40 (2015) 115-118.

[7] Y.N. Kulchin, O.B. Vitrik, A.V. Dyshlyuk, et al., Analysis of surface plasmon resonance in bent single-mode waveguides with metal-coated cladding by eigenmode expansion method, Optics Express. 22 (2014) 22196-22201.

[8] X.Zhang, P. Liang, Y. Wang, et al., Cascaded distributed multichannel fiber SPR sensor based on gold film thickness adjustment approach, Sensors and Actuators A physical. 267 (2017) 526–531 .

[9] X.F. Wang, J.Q. Zhang, k. Tian, et al., Investigation of a novel SMS fiber based planar multimode waveguide and its sensing performance, Optics Express. 2018 (26) 26534-26543.

[10] A.A. Rifat, R. Ahmed, A.K. Yetisen, et al., Photonic crystal fiber based plasmonic sensors, Sensors and Actuators B Chemical. 243 (2017) 311-325.

[11] Y. T. Chen, Y. Y.Liao, C.C. Chen, et al., Surface plasmons coupled two-dimensional photonic crystal biosensors for Epstein-Barr virus protein detection, Sensors and Actuators B Chemical. 291 (2019) 81-88.

[12] M. Piliarik, J. Homola, Z. Manková, et al., Surface plasmon resonance sensor based on a single-mode polarization-maintaining optical fiber, Sensors and Actuators B Chemical. 90 (2003) 236-242.

[13] Y. Al-Qazwini, A.S.M. Noor, Z. Al-Qazwini, et al., Refractive index sensor based on SPR in

symmetrically etched plastic optical fibers, Sensors and Actuators A Physical, 246 (2016) 136-139.

[14] B.H. Liu, Y.X. Jiang, X.S. Zhu, et al., Hollow fiber surface plasmon resonance sensor for the detection of liquid with high refractive index, Optics Express. 21 (2013) 32349-32357.

[15] H. Zhang, Y. Chen, H. Wang, et al., Titanium dioxide nanoparticle modified plasmonic interface for enhanced refractometric and biomolecular sensing, Optics Express. 26 (2018) 33226.

[16] S. Shukla, N.K. Sharma, V. Sajal, Sensitivity enhancement of a surface plasmon resonance based fiber optic sensor using ZnO thin film: a theoretical study, Sensors and Actuators B Chemical. 206 (2015) 463-470.

[17] H.M. Kim, J.H. Park, S.K.Lee, et al., Fiber optic sensor based on ZnO nanowires decorated by Au nanoparticles for improved plasmonic biosensor, Scientific Reports. 9 (2019) 15605.

[18] K. Liu , M. Xue , J. Jiang, et al., Theoretical modeling of a coupled plasmon waveguide resonance sensor based on multimode optical fiber, Optics Communications. 410 (2018) 552-558.

[19] A.A. Rifat, G.A. Mahdiraji, Y.M. Sua, et al., Highly sensitive multi-core flat fiber surface plasmon resonance refractive index sensor, Optics Express. 24 (2016) 2485-2495.

[20] S. Zeng, S. Hu, J. Xia, et al., Graphene–$MoS_2$ hybrid nanostructures enhanced surface plasmon resonance biosensors, Sensors and Actuators B Chemical. 207 (2015) 801-810.

[21] Y. Cai, W. Li, Y. Feng, et al., Sensitivity enhancement of $WS_2$-coated SPR-based optical fiber biosensor for detecting glucose concentration, Chinese Physics B. 29 (2020) 110701.

[22] H. Wang, H. Zhang, J.L. Dong, et al., Sensitivity-enhanced surface plasmon resonance sensor utilizing a tungsten disulfide ($WS_2$) nanosheets overlayer, Photonics Research. 6 (2018) 485-491.

[23] K. Liu, J.H. Zhang, J.F. Jiang, et al., $MoSe_2$-Au Based Sensitivity Enhanced Optical Fiber Surface Plasmon Resonance Biosensor for Detection of Goat-Anti-Rabbit IgG, IEEE Access. 8 (2020) 660-668.

[24] Y. Zhu, S.Murali, W. Cai, et al., Graphene and graphene oxide: synthesis, properties, and applications, Advanced Materials. 22 (2010) 3906-3924.

[25] F.Yan, Y.Zhang, S. Zhang, et al., Carboxyl-modified graphene for use in an immunoassay for the illegal feed additive clenbuterol using surface plasmon resonance and electrochemical impedance spectroscopy, Microchimica Acta. 182 (2015) 855-862.

[26] F.M. Wang, Z. Sun, C. Liu, et al., A Highly Sensitive Dual-Core Photonic Crystal Fiber Based on a Surface Plasmon Resonance Biosensor with Silver-Graphene Layer, Plasmonics. 2017 (12) 1847-1853.

[27] C. Zhang, Z. Li , S.Z. Jiang, et al., U-bent fiber optic SPR sensor based on graphene/AgNPs, Sensors and Actuators B Chemical. 251 (2017) 127-133.

[28] N.J. Kumar, J. Rajan, Numerical simulation on the performance analysis of a graphene-coated optical fiber plasmonic sensor at anti-crossing, Applied Optics. 56 (2017) 3510-3517.

[29] N. Luan, R. Wang, W. Lv, J. Yao, et al., Surface plasmon resonance sensor based on D-shaped microstructured optical fiber with hollow core, Optics Express. 23 (2015) 8576–8582.
[30] L. Coelho, J. Almeida, J.L. Santos, et al., Sensing structure based on surface plasmon resonance in chemically etched single mode optical fibres, Plasmonics. 10 (2015) 319-327.
[31] J.C. Shin , M.S. Yoon, Y.G. Han, et al., Relative humidity sensor based on an optical microfiber knot resonator with a polyvinyl alcohol overlay, Journal of Lightwave Technology. 34 (2015) 4511-4515.
[32] A.K. Sharma, B.D. Gupta, On the performance of different bimetallic combinations in surface plasmon resonance based fiber optic sensors, Journal of Applied Physics. 101 (2007) 093111.
[33] J.R. Devore, Refractive Indices of Rutile and Sphalerite, Journal of the Optical Society of America. 41 (1951) 266-266.
[34] M. Bruna, S. Borini, Optical constants of graphene layers in the visible range, Applied Physics Letters. 94 (2009) 031901.
[35] H. Song, Q. Wang, W.M. Zhao, et al., A novel SPR sensor sensitivity-enhancing method for immunoassay by inserting $MoS_2$ nanosheets between metal film and fibe. Optics and Lasers in Engineering. 132 (2020) 106135.
[36] X.C. Yang, Y. Lu, B.L. Liu, et al., Analysis of Graphene-Based Photonic Crystal Fiber Sensor Using Birefringence and Surface Plasmon Resonance, Plasmonics. 12 (2017) 1-8.
[37] Q. Bao, K.P. Loh, Graphene photonics, plasmonics, and broadband optoelectronic devices. Acs Nano. 6 (2012) 3677-3694.
[38] F.H.L. Koppens, D.E. Chang, F.J.G.D. Abajo, et al., Graphene plasmonics: a platform for strong light-matter interactions, Nano Letters. 11 (2011) 3370-3377.

**Figure**

**Fig.1.** Tapered fiber structure diagram and cross-sectional view of the sensing area.

**Fig.2.** (a)z=0 electric field intensity distribution diagram in cross section.

(b) one-dimensional amplitude distribution diagram in cross section.

**Fig.3.** Transmittance spectra of sensors with different silver thickness.

**Fig.4.** (a) When the silver film thickness is 40 nm, the spectrum of the sensor (b)When the silver film thickness is 40 nm, the sensitivity of the sensor.

**Fig.5.** (a)Variation of SPR resonance wavelength with graphene layers and external refractive index (b)The external refractive index is 1.37, and the sensitivity and FWHM vary with the number of graphene layers.

**Fig.6.** SPR transmission spectra under different $TiO_2$ thicknesses, RI=1.37

(a)0-25 nm (b)20 nm (c)25 nm.

**Fig.7.** The relationship between resonant peak and analyte refractive index under different $TiO_2$ thickness.

**Fig.8.** The relationship between sensitivity and refractive index of analyte under different $TiO_2$ layer thickness.

**Fig.9.** SPR resonance spectrum (a)40 nm Ag (b)15-layer graphene/40 nm Ag (c)40 nm Ag/20 nm $TiO_2$ (d)15-layer graphene/40 nm Ag/20 nm $TiO_2$.

**Fig.10.** RI=1.32, electric field intensity and amplitude distribution diagram in cross section (a)40 nm Ag (b)15-layer graphene/40 nm Ag (c)15-layer graphene/40 nm Ag/20 nm $TiO_2$.

**Fig.11.** The electric field intensity distribution diagram of the tapered fiber SPR sensor with 15-layer graphene/40 nm Ag/20 nm $TiO_2$ structure under different analyte refractive index.

**Table**

**Table 1** Sensitivity, FWHM and FOM of sensors with different graphene layers and a refractive index of 1.37.

**Table 2** Sensitivity comparison of SPR sensor with 15 layers of graphene and without graphene.

**Table 3** Comparison of sensitivity and detection range of SPR sensors with different structures.

**Table 4** Sensitivity and FWHM of SPR sensors with different structures at external RI = 1.36.

**Fig.1**

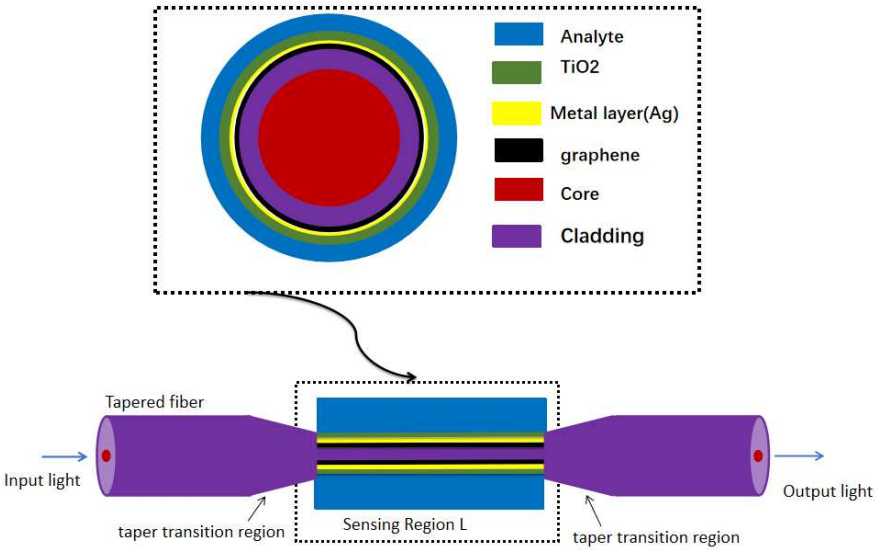
Analyte
TiO2
Metal layer(Ag)
graphene
Core
Cladding
Tapered fiber
Input light
taper transition region
Sensing Region L
taper transition region
Output light

**Fig.2**

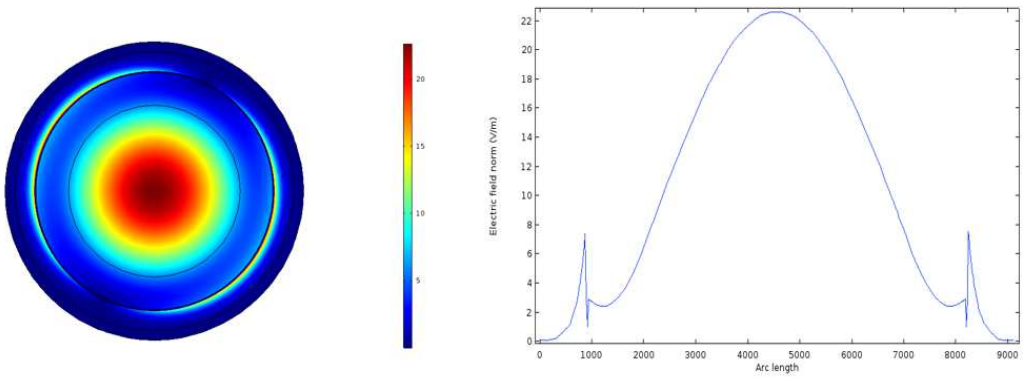
Electric field norm (V/m)
Arc length

(a) (b)

**Fig.3**

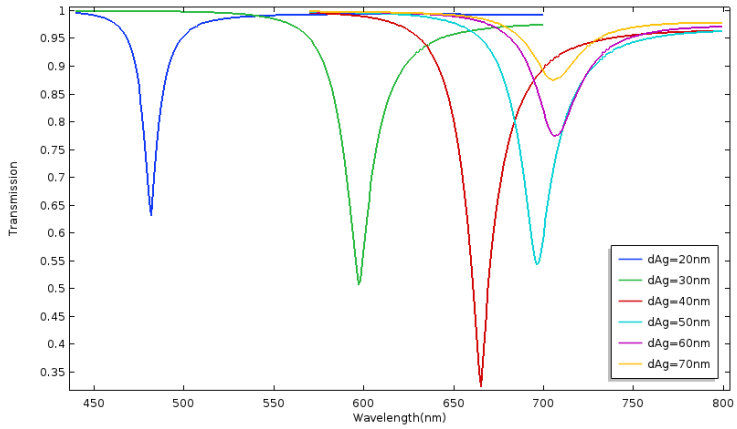
Transmission
Wavelength(nm)
dAg=20nm
dAg=30nm
dAg=40nm
dAg=50nm
dAg=60nm
dAg=70nm

**Fig.4**

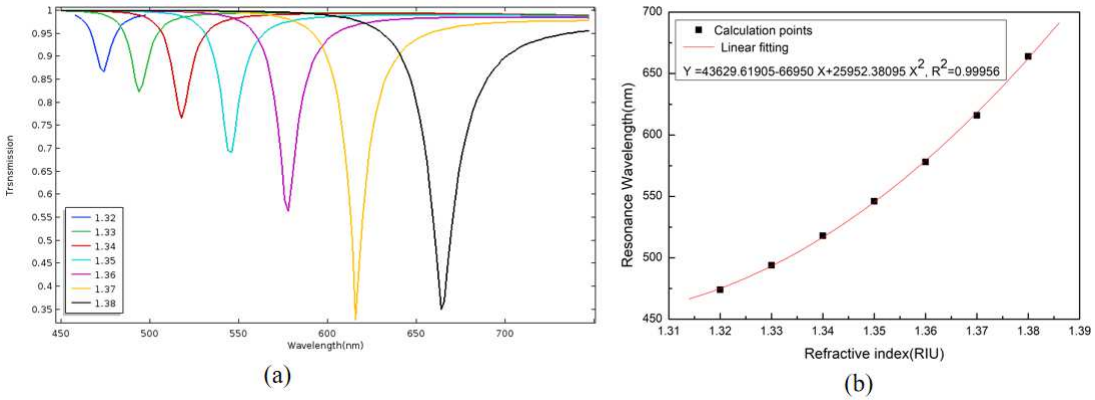
Transmission
Wavelength(nm)
1.32
1.33
1.34
1.35
1.36
1.37
1.38
Calculation points
Linear fitting
Y =43629.61905-66950 X+25952.38095 X2, R2=0.99956
Resonance Wavelength(nm)
Refractive index(RIU)

(a) (b)

**Fig.5**

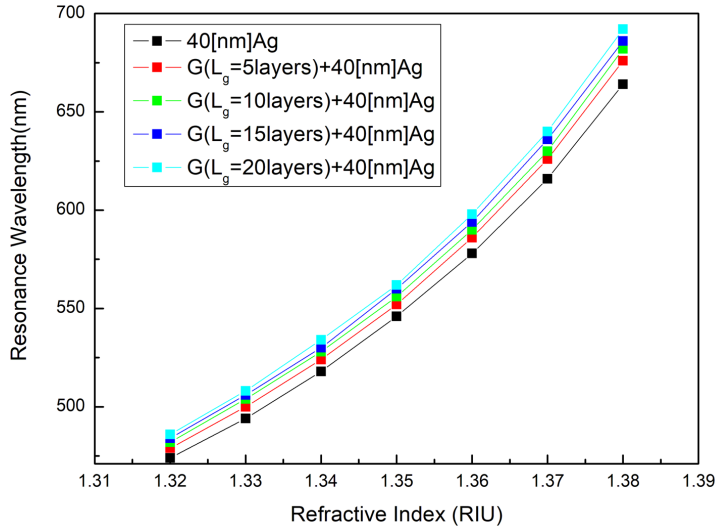
40[nm]Ag
G(Lg=5layers)+40[nm]Ag
G(Lg=10layers)+40[nm]Ag
G(Lg=15layers)+40[nm]Ag
G(Lg=20layers)+40[nm]Ag
Resonance Wavelength(nm)
Refractive Index (RIU)
700
650
600
550
500
1.31
1.32
1.33
1.34
1.35
1.36
1.37
1.38
1.39

(a)

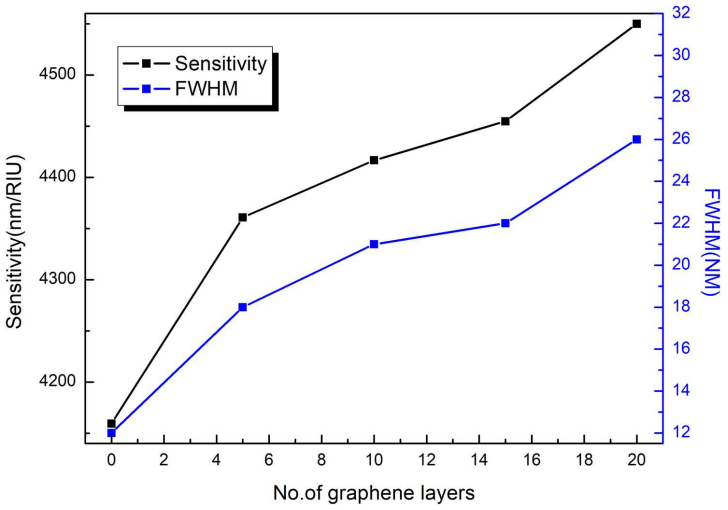
Sensitivity
FWHM
Sensitivity(nm/RIU)
FWHM(NM)
No.of graphene layers
4500
4400
4300
4200
32
30
28
26
24
22
20
18
16
14
12
0
2
4
6
8
10
12
14
16
18
20

(b)

**Fig.6**

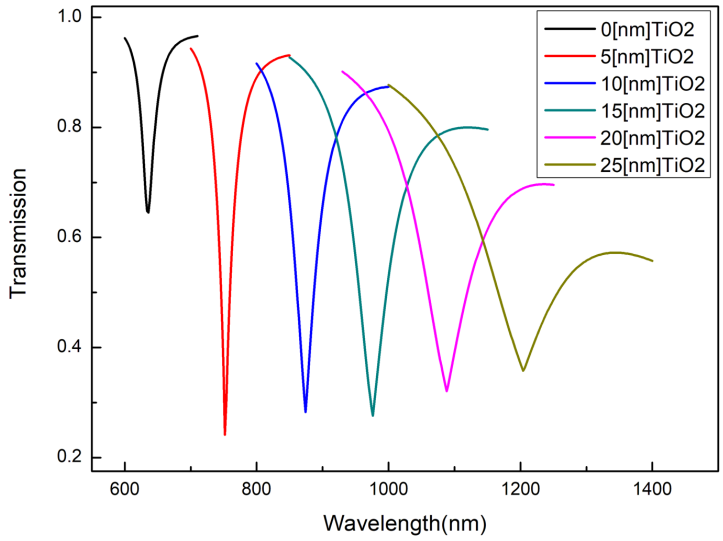
0[nm]TiO2
5[nm]TiO2
10[nm]TiO2
15[nm]TiO2
20[nm]TiO2
25[nm]TiO2
Transmission
Wavelength(nm)
1.0
0.8
0.6
0.4
0.2
600
800
1000
1200
1400

(a)

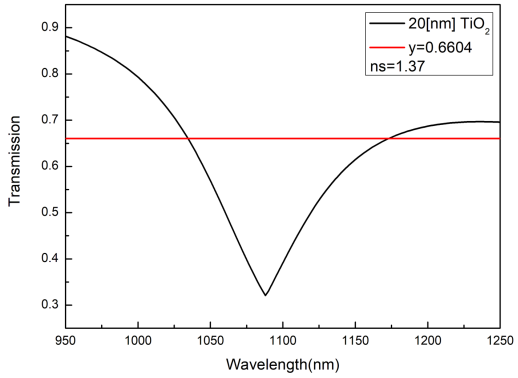
20[nm] TiO2
y=0.6604
ns=1.37
Transmission
Wavelength(nm)
0.9
0.8
0.7
0.6
0.5
0.4
0.3
950
1000
1050
1100
1150
1200
1250

(b)

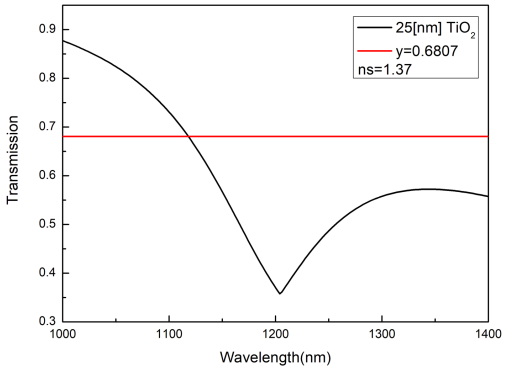
25[nm] TiO2
y=0.6807
ns=1.37
Transmission
Wavelength(nm)
0.9
0.8
0.7
0.6
0.5
0.4
0.3
1000
1100
1200
1300
1400

(c)

**Fig.7**

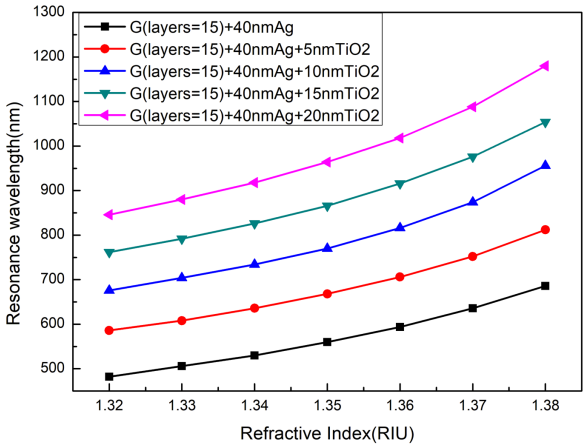
G(layers=15)+40nmAg
G(layers=15)+40nmAg+5nmTiO2
G(layers=15)+40nmAg+10nmTiO2
G(layers=15)+40nmAg+15nmTiO2
G(layers=15)+40nmAg+20nmTiO2
Resonance wavelength(nm)
Refractive Index(RIU)
1300
1200
1100
1000
900
800
700
600
500
1.32
1.33
1.34
1.35
1.36
1.37
1.38

**Fig.8**

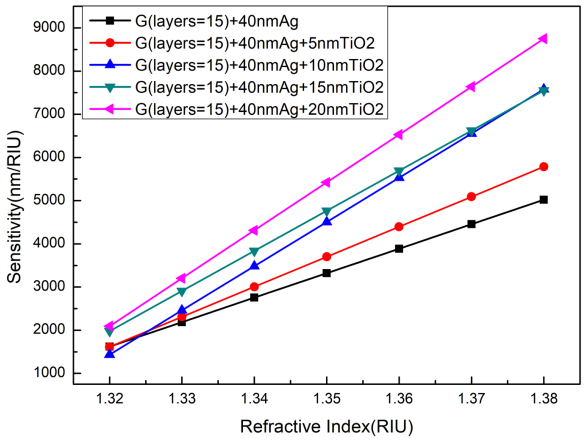
G(layers=15)+40nmAg
G(layers=15)+40nmAg+5nmTiO2
G(layers=15)+40nmAg+10nmTiO2
G(layers=15)+40nmAg+15nmTiO2
G(layers=15)+40nmAg+20nmTiO2
Sensitivity(nm/RIU)
Refractive Index(RIU)
9000
8000
7000
6000
5000
4000
3000
2000
1000
1.32
1.33
1.34
1.35
1.36
1.37
1.38

**Fig.9**

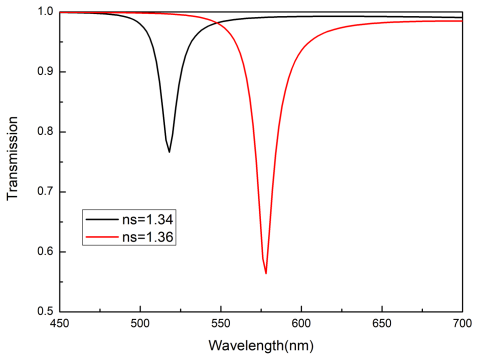
Transmission
Wavelength(nm)
ns=1.34
ns=1.36

(a)

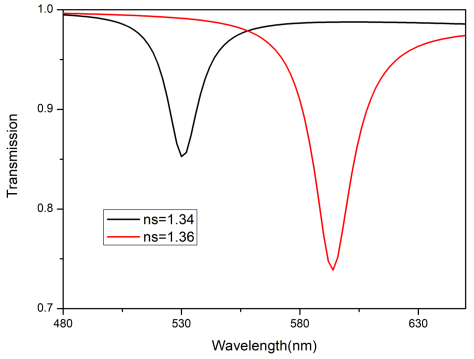
Transmission
Wavelength(nm)
ns=1.34
ns=1.36

(b)

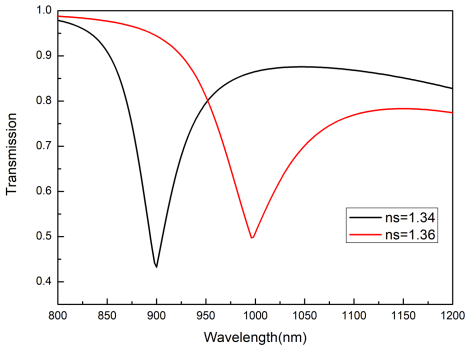
Transmission
Wavelength(nm)
ns=1.34
ns=1.36

(c)

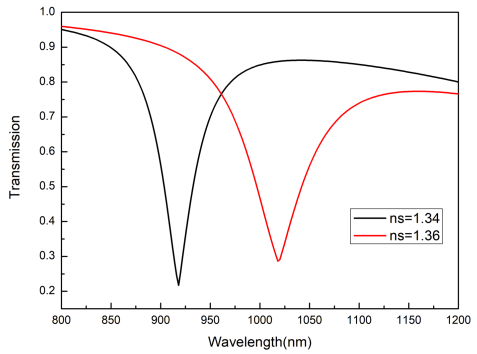
Transmission
Wavelength(nm)
ns=1.34
ns=1.36

(d)

**Fig.10**

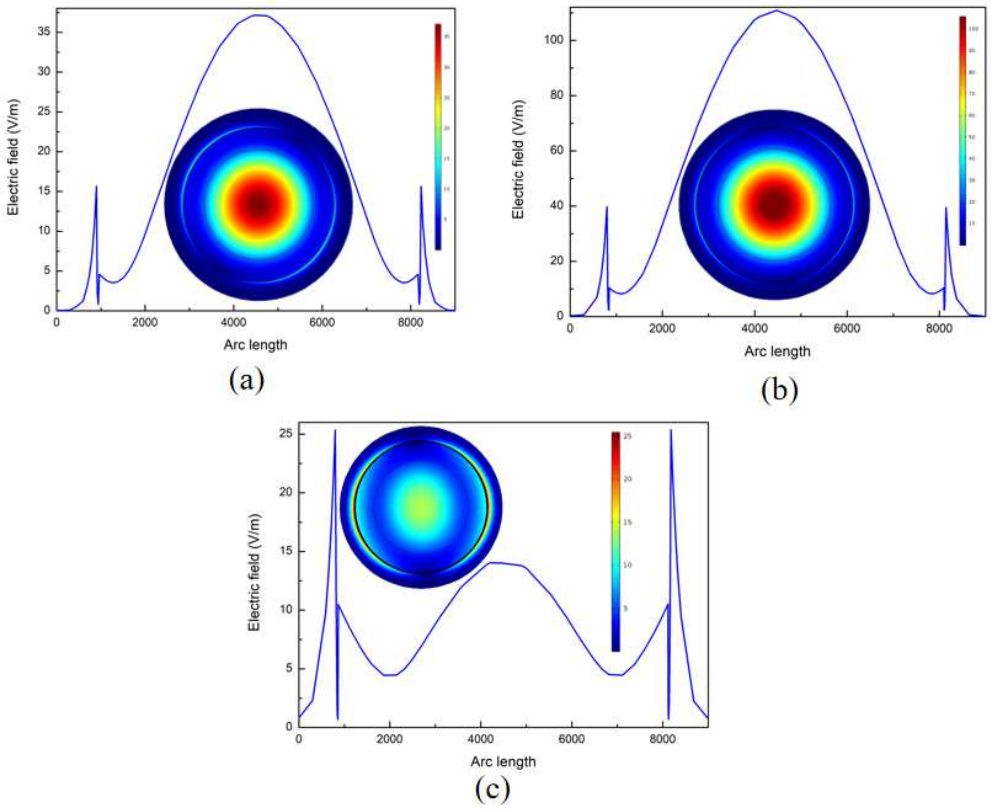
Electric field (V/m)
Arc length
(a)
Electric field (V/m)
Arc length
(b)
Electric field (V/m)
Arc length
(c)

**Fig.11**

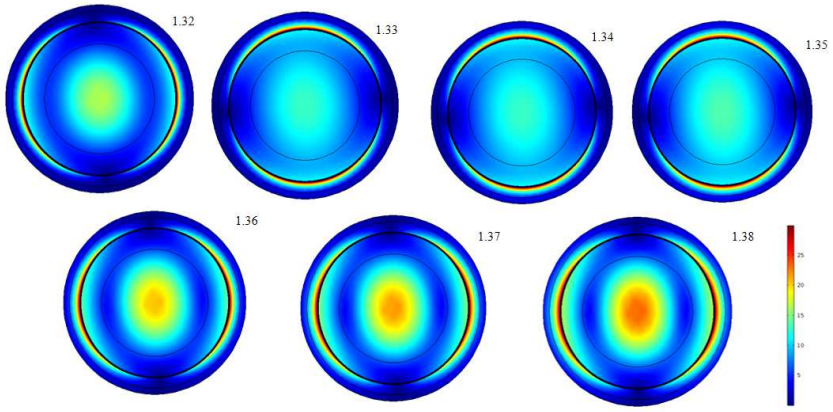
1.32
1.33
1.34
1.35
1.36
1.37
1.38

**Table 1**

| No.of graphene layers | Sensitivity(nm/RI) | FWHM(nm) | FOM($RIU^{-1}$) |
|---|---|---|---|
| **0** | 4159.0 | 12 | 346.5 |
| **5** | 4360.7 | 18 | 242.2 |
| **10** | 4416.6 | 21 | 210.3 |
| **15** | 4454.7 | 22 | 202.5 |
| **20** | 4549.9 | 26 | 174.9 |

**Table 2**

| No.of graphene layers | Sensitivity (nm/RIU) (RI = 1.32) | Sensitivity (nm/RIU) (RI=1.34) | Sensitivity (nm/RIU) (RI = 1.36) | Sensitivity (nm/RIU) (RI = 1.38) |
|---|---|---|---|---|
| **0** | 1564.3 | 2602.4 | 3640.47 | 4678.6 |
| **15** | 1621.4 | 2754.8 | 3888.1 | 5021.4 |

**Table 3**

| Sensor Configuration | Detection range(RIU) | Sensitivity(nm/RIU) | Reference |
|---|---|---|---|
| Ag/$TiO_2$ | 1.333-1.403 | 1048.48 | [18] |
| Ag/ZnO | 1.30-1.37 | 3054 | [16] |
| $MoS_2$/Au | 1.33-1.36 | 6184.4 | [35] |
| Ag/Graphene PCF | 1.33-1.35 | 2520 | [36] |
| Ag/Graphene | 1.34-1.37 | 6800 | [28] |
| Graphene/Ag/$TiO_2$ | 1.32-1.38 | 8570 | This paper |

**Table4**

| SPR sensor structure | $\Delta\lambda$ (nm) | FWHM(nm) | Sensitivity(nm/RIU) |
|---|---|---|---|
| 40 nm Ag | 60 nm | 14 nm | 3000 nm/RIU |
| 15-layer graphene/40 nm Ag | 64 nm | 20 nm | 3200 nm/RIU |
| 40 nm Ag/20 nm $TiO_2$ | 96 nm | 115 nm | 4800 nm/RIU |
| 15layers graphene/40 nm Ag/20 nm $TiO_2$ | 100 nm | 84 nm | 5000 nm/RIU |

# Figures

**Fig.1**

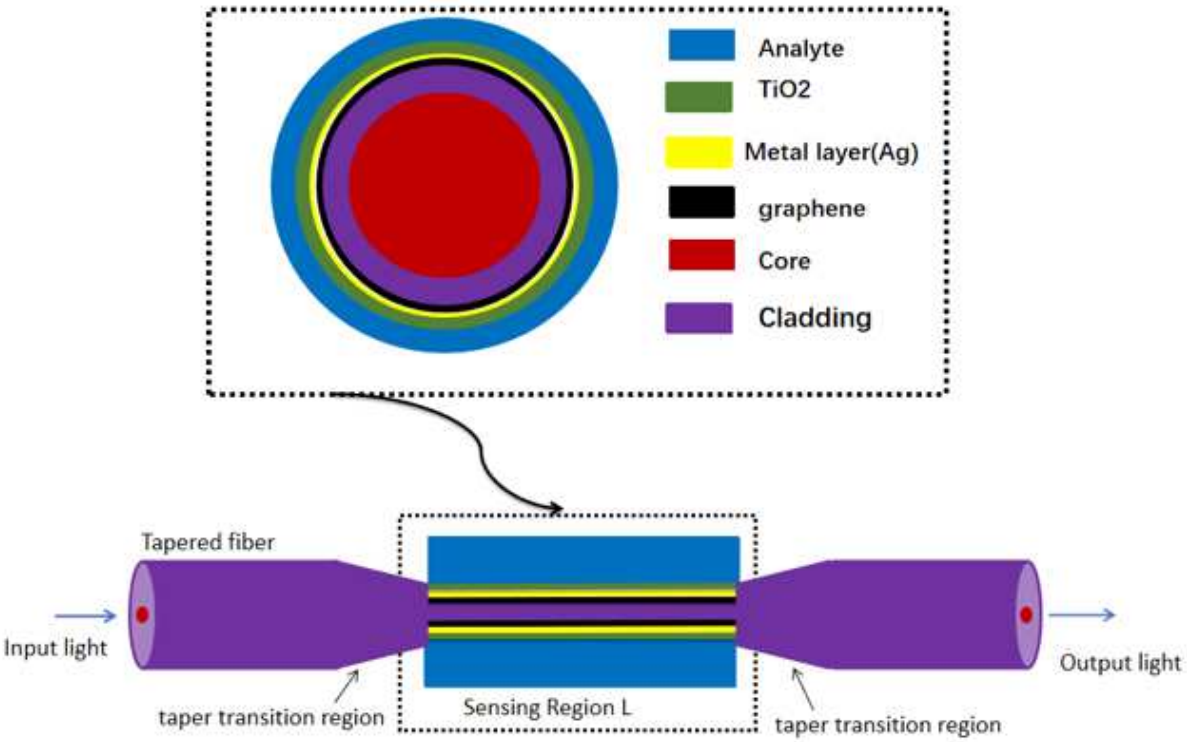


**Figure 1**

Tapered fiber structure diagram and cross-sectional view of the sensing area.

**Fig.2**

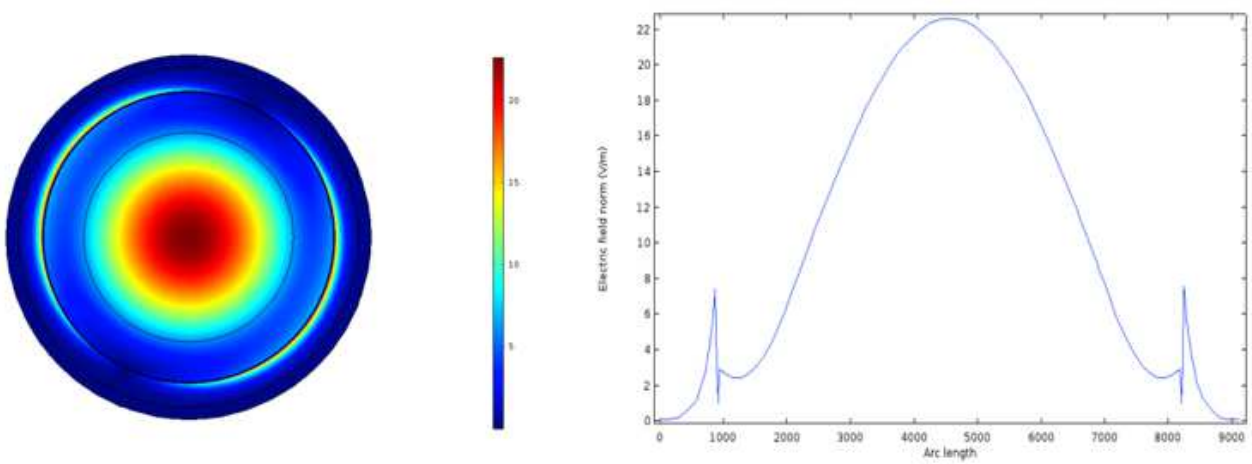


**Figure 2**

(a)z=0 electric field intensity distribution diagram in cross section. (b) one-dimensional amplitude distribution diagram in cross section.

**Fig.3**

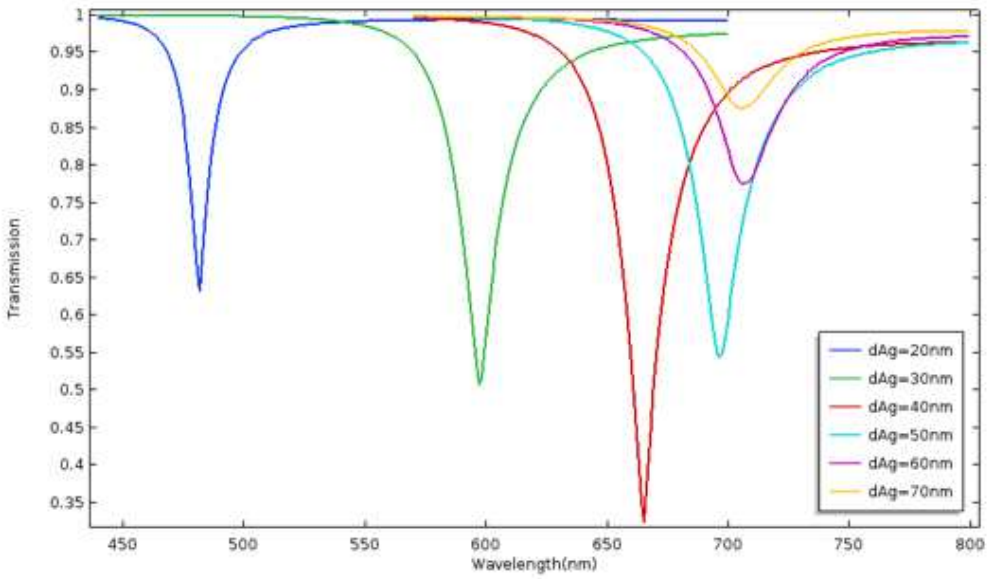


**Figure 3**

Transmittance spectra of sensors with different silver thickness.

**Fig.4**

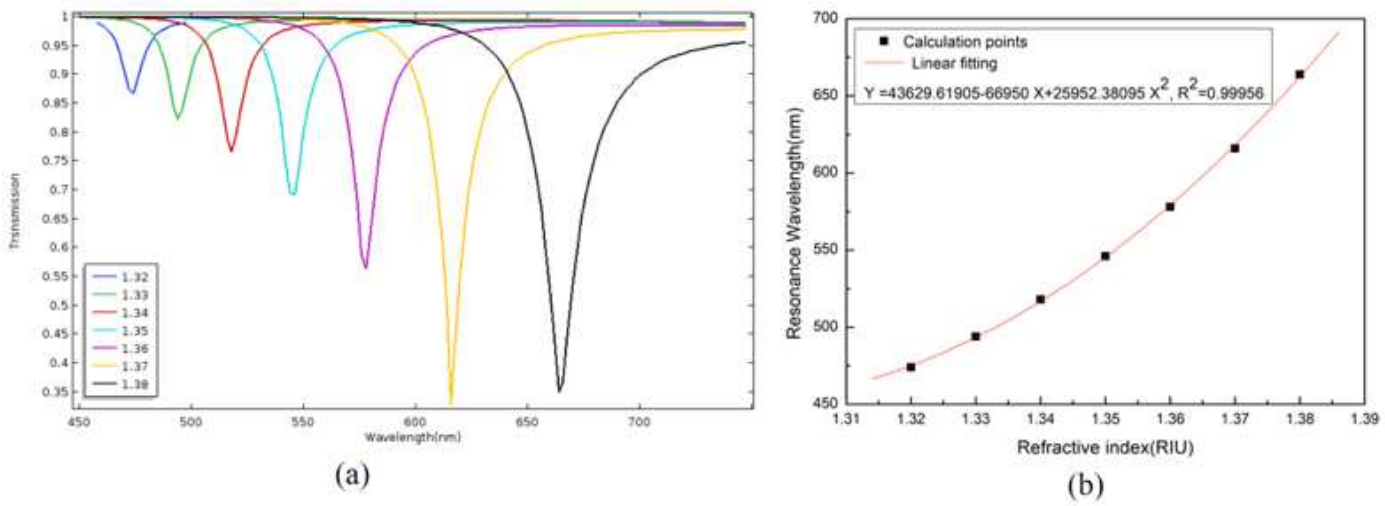


## Figure 4

(a) When the silver film thickness is 40 nm, the spectrum of the sensor (b)When the silver film thickness is 40 nm, the sensitivity of the sensor.

**Fig.5**

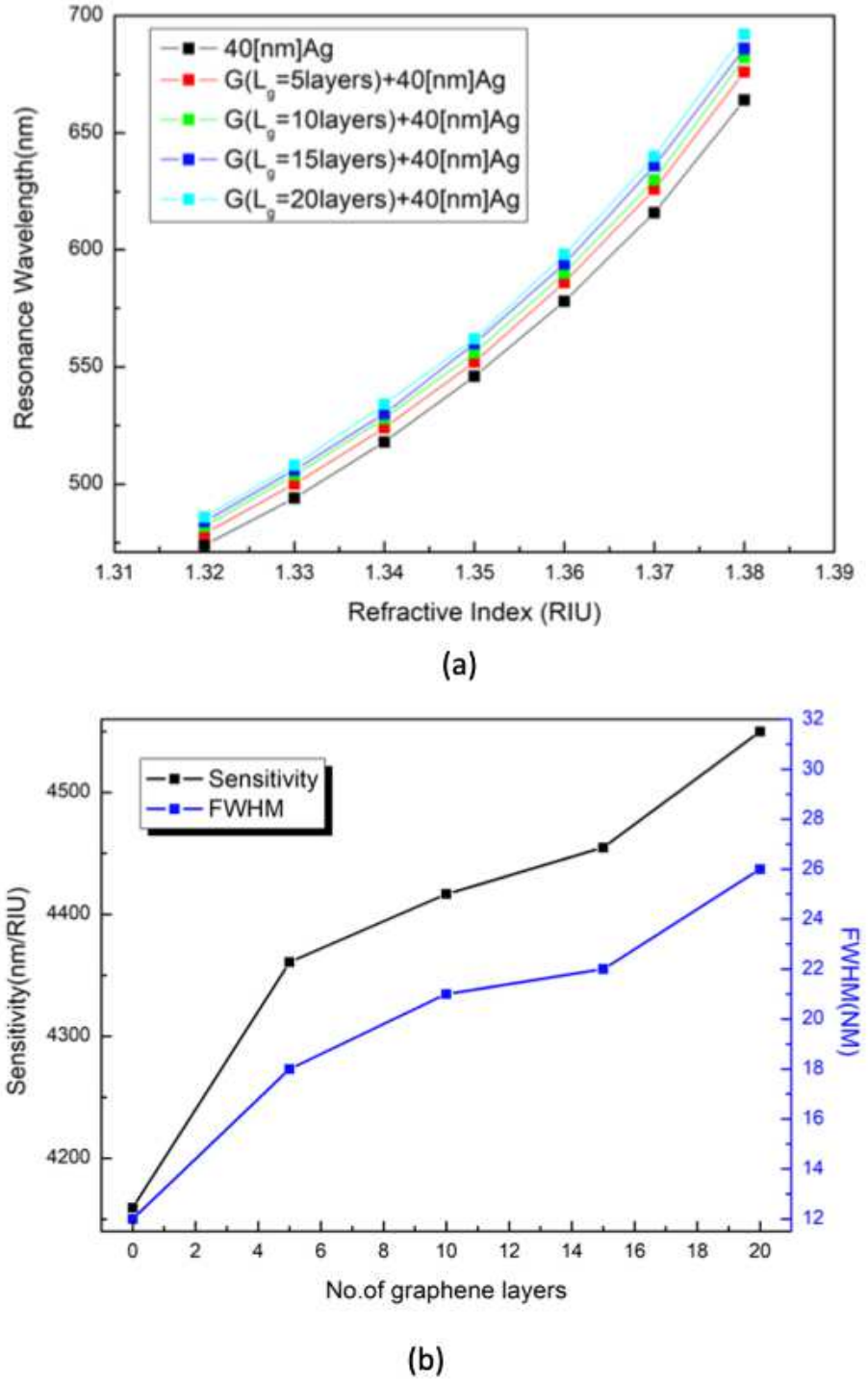


## Figure 5

(a)Variation of SPR resonance wavelength with graphene layers and external refractive index (b)The external refractive index is 1.37, and the sensitivity and FWHM vary with the number of graphene layers.

**Fig.6**

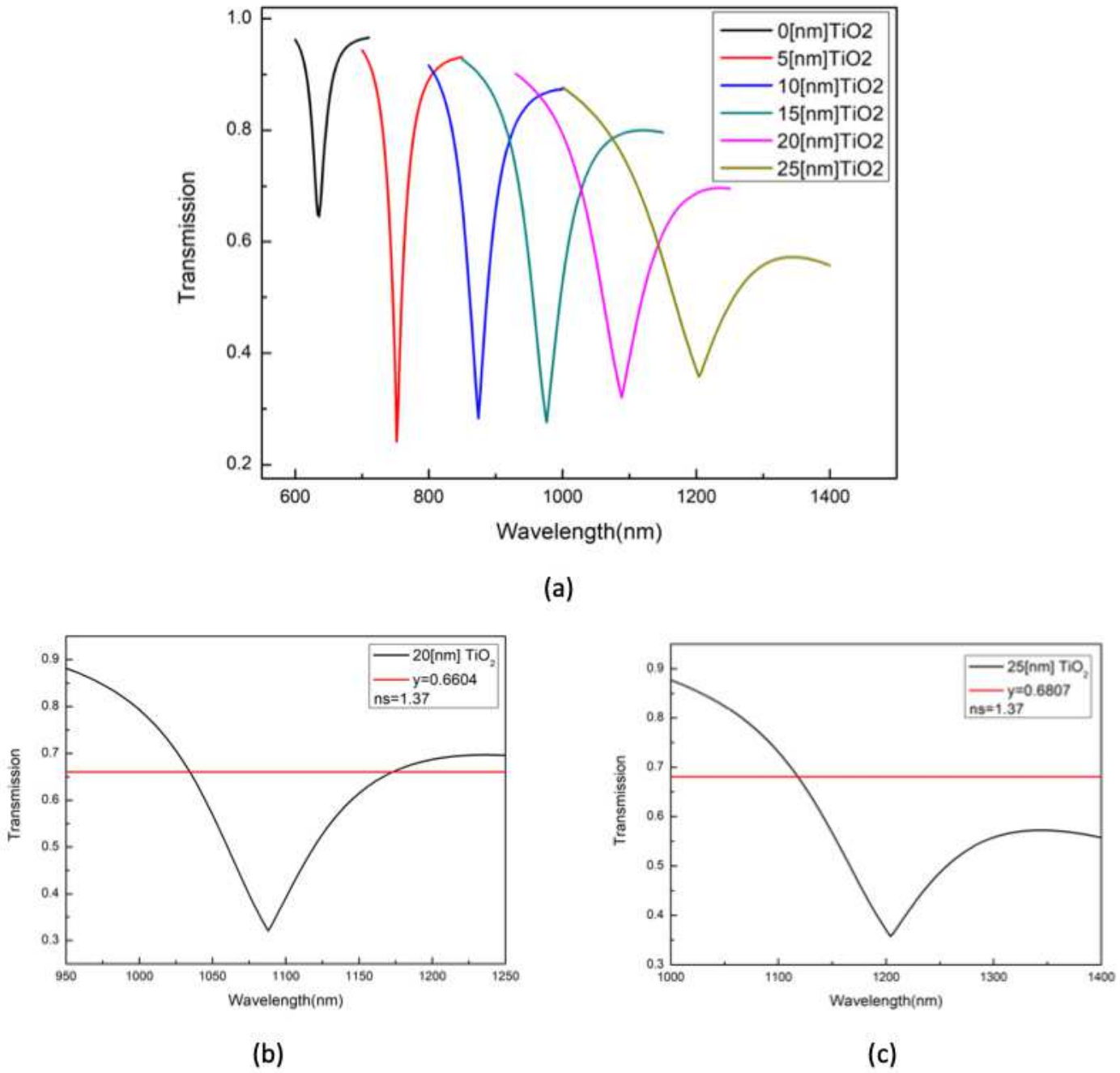


## Figure 6

SPR transmission spectra under different TiO2 thicknesses, RI=1.37 (a)0-25 nm (b)20 nm (c)25 nm.

**Fig.7**

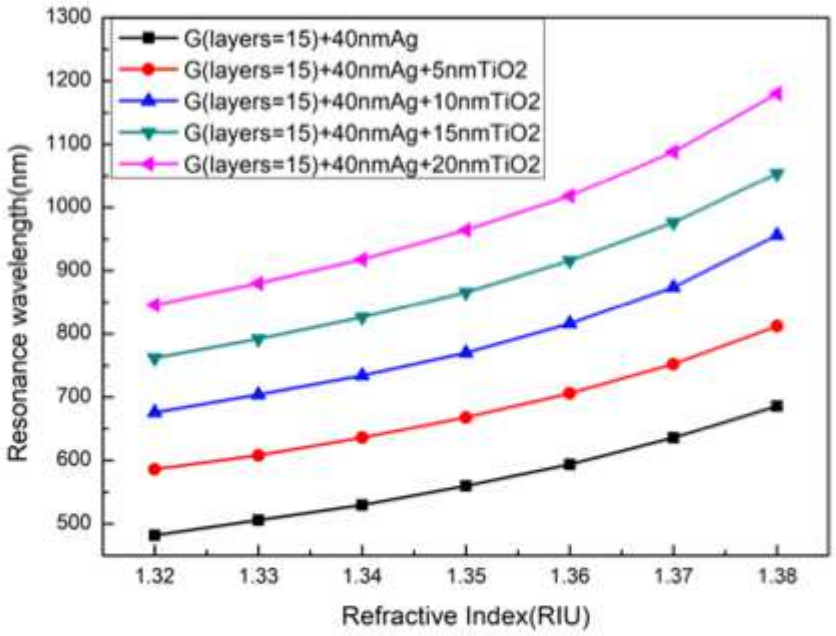


**Figure 7**

The relationship between resonant peak and analyte refractive index under different TiO2 thickness.

**Fig.8**

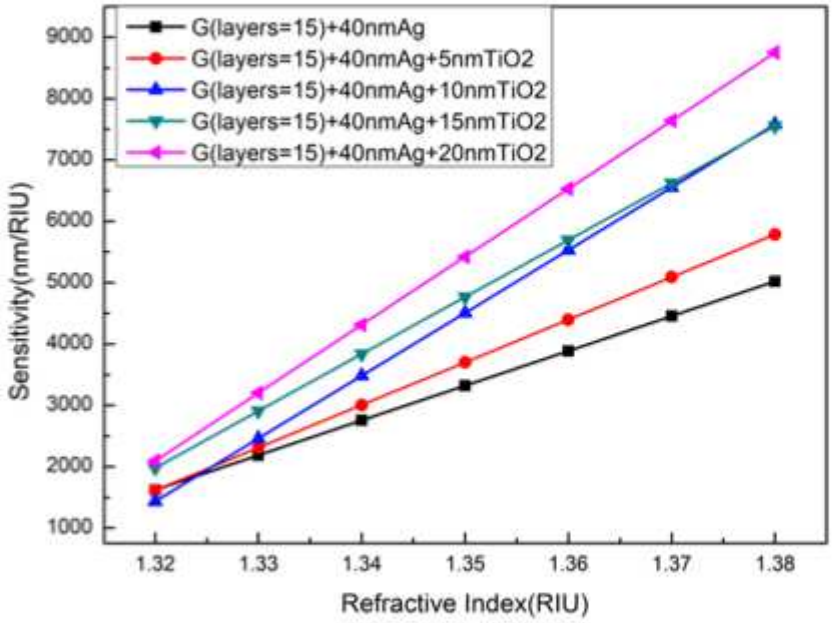


## Figure 8

The relationship between sensitivity and refractive index of analyte under different TiO2 layer thickness.

**Fig.9**

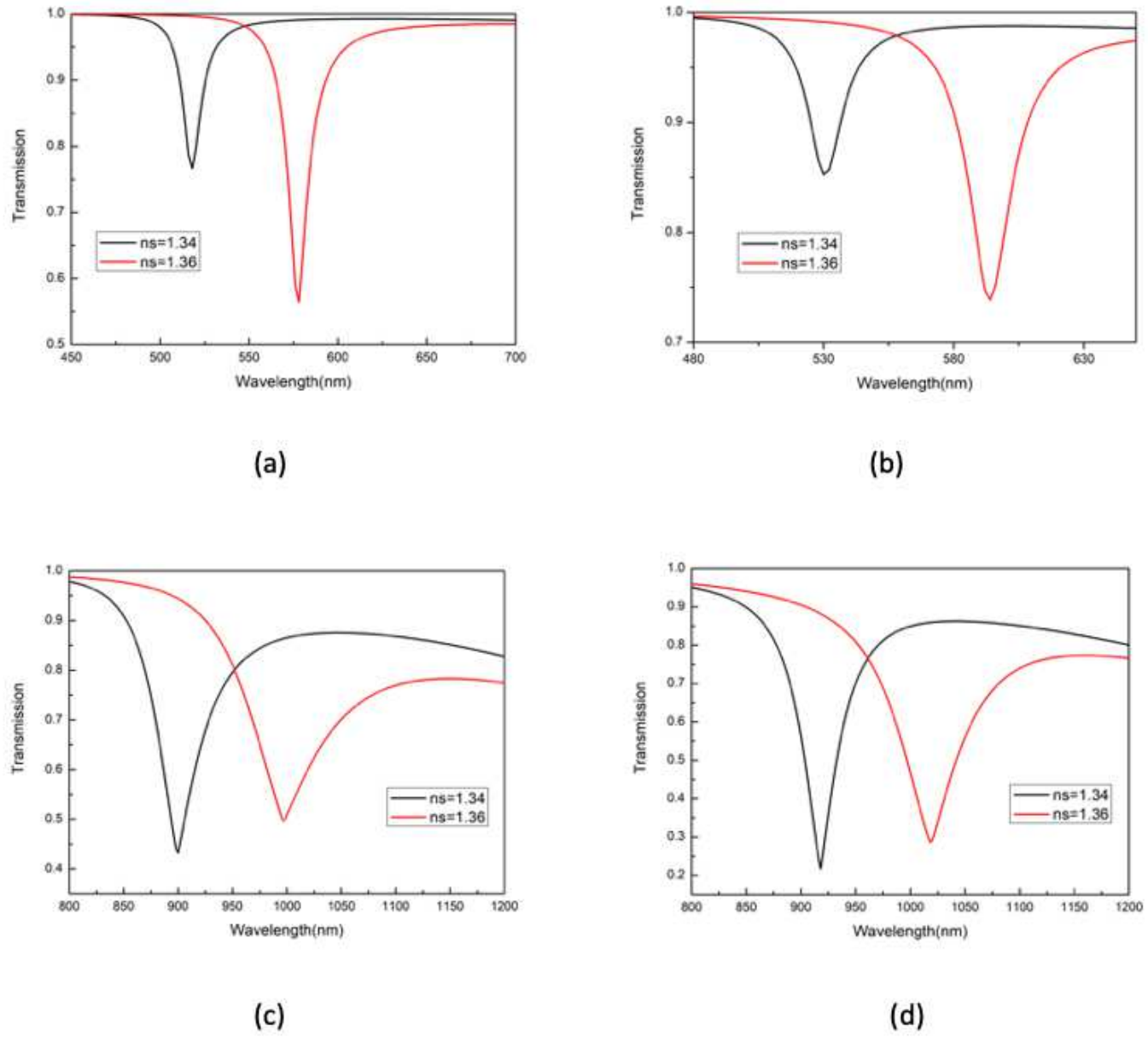


## Figure 9

SPR resonance spectrum (a)40 nm Ag (b)15-layer graphene/40 nm Ag (c)40 nm Ag/20 nm TiO2 (d)15-layer graphene/40 nm Ag/20 nm TiO2.

**Fig.10**

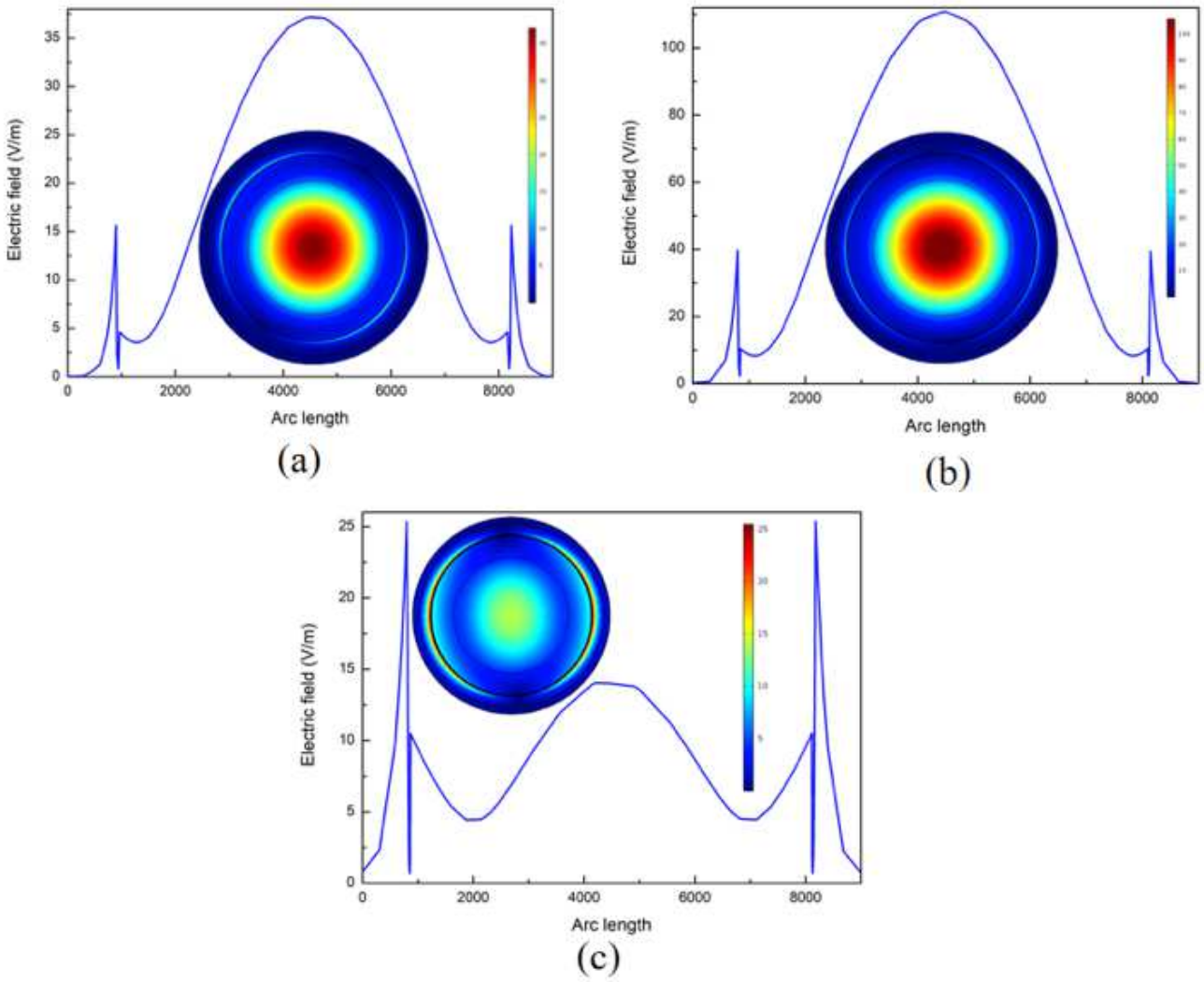


## Figure 10

RI=1.32, electric field intensity and amplitude distribution diagram in cross section (a)40 nm Ag (b)15-layer graphene/40 nm Ag (c)15-layer graphene/40 nm Ag/20 nm TiO2.

**Fig.11**

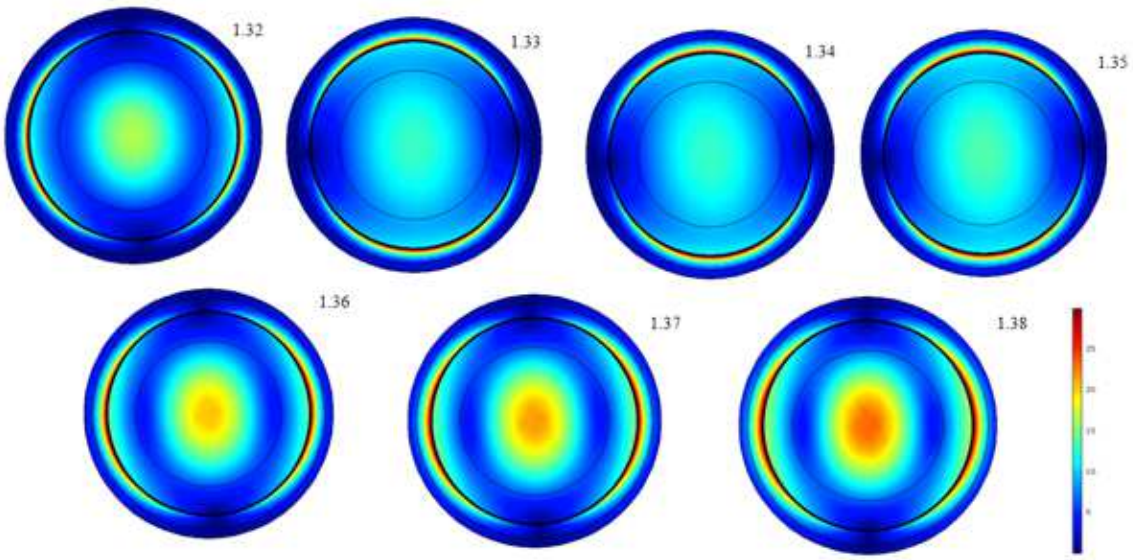




**Figure 11**

The electric field intensity distribution diagram of the tapered fiber SPR sensor with 15-layer graphene/40 nm Ag/20 nm TiO2 structure under different analyte refractive index.